Catalysis Science & Technology

ROYAL SOCIETY OF CHEMISTRY

PAPER

View Article Online
View Journal | View Issue

Cite this: *Catal. Sci. Technol.*, 2025, 15, 3075

Immobilization of a chiral rhodium catalyst on carbon nanotubes *via* non-covalent interaction for heterogeneous asymmetric hydrogenation†

Zinnia Arora,[ab] Vasile I. Pârvulescu,[b] Karine Philippot,[a] Jérôme Durand[a] and Maryse Gouygou*[a]

Received 2nd December 2024,
Accepted 21st March 2025

DOI: 10.1039/d4cy01457j

rsc.li/catalysis

A new chiral rhodium complex containing a diphosphine ligand with a pyrene tag, Rh-(2*S*,4*S*)-PPM-pyrene, was synthesized. Its immobilization was achieved through non-covalent π–π stacking interaction between pyrene units of the ligand and multiwalled carbon nanotubes, leading to a hybrid material that was characterized by a set of analysis techniques. Strong adsorption of the complex onto the CNTs enabled an asymmetric hydrogenation of dimethyl itaconate under heterogeneous conditions. This hybrid catalyst showed reduced activity and enantioselectivity compared to its free complex but exhibited good stability for recycling.

Introduction

Homogeneous asymmetric catalysis has made significant progress due to the efforts in the ligand design, catalyst development, and powerful rationalization of the metal–ligand–solvent systems. However, product separation and catalyst recycling remain to be two major issues that need solutions before development of any catalytic process. Recent inputs in asymmetric catalysis involve the heterogenization of chiral complexes by immobilization on different supports. The immobilization of homogeneous chiral complexes can allow combining the advantages of both the homogeneous catalysts (high catalytic activity and enantioselectivity) and the heterogeneous catalysts (easy separation and recycling of the expensive chiral catalytic systems). Also, these supported catalysts are particularly interesting for: i) clean reactions leading to metal-free organic products, and ii) applications in flow catalysis using continuous fixed bed reactors.

Although the most common immobilization methods involve covalent anchoring of the enantioselective catalysts, their non-covalent immobilization has been the subject of exhaustive reviews for almost 15 years.[1a–g] Most of them employ electrostatic, acid–base, hydrophobic or coordination interactions, adsorption or entrapment strategies. More recently, weak interactions, such as the π–π interactions, have been shown to provide robust immobilizations.[2]

As an additional advantage the π–π interactions with carbon supports do not require complex procedures since no modification of the support is necessary. However, to the best of our knowledge, only a few reports of Rh-catalysts immobilized by π–π stacking onto carbon materials have been described to date for asymmetric hydrogenation reactions.

Román-Martínez' group[3] reported the immobilization of a 1,2-bis [(2*R*,5*R*)-2,5-dimethylphospho-lano]benzene(1,5-cyclooctadiene)rhodium(I)tetrafluoroborate complex by π–π interactions between the phenylene group of the (*R*,*R*)-RhDuphos ligand and the surface of demineralized CNTs. This catalyst exhibited a rather poor enantioselectivity (4.5%) in the asymmetric hydrogenation of 2-methyl-acetamido-acrylate (MAA) due to the low stability under the catalytic reaction conditions. The same authors[4] studied the heterogenization of the chiral (*R*,*R*)-RhDuphos Rh-complex on carbon black using L-tryptophan (Trp) as an anchoring ligand. This approach relies on: i) a π–π interaction between the support and the aromatic moiety of Trp and ii) complexation of the amino acid moiety of Trp on the cationic Rh-complex leading to an efficient adsorption onto the carbon surface and a high activity but only a moderate enantioselectivity (43–60%) for the asymmetric hydrogenation of 2-methy-lacetamido-acrylate.

On the other side, pyrene is confirmed as the polyaromatic moiety of choice to generate π–π stacking interactions with a sp^2 graphitic carbon network. Further, the adsorption of pyrene is a reversible process that can be controlled, at least partially, either by the temperature or by

[a] *Laboratoire de Chimie de Coordination du CNRS, Université de Toulouse, UPS, Toulouse-INP, 205 route de Narbonne, BP 44099, F-31077 Toulouse Cedex 4, France. E-mail: karine.philippot@lcc-toulouse.fr, maryse.gouygou@lcc-toulouse.fr*
[b] *Department of Organic Chemistry, Biochemistry and Catalysis, University of Bucharest, 4-12 Regina Elisabeta Avenue, S3, 030018, Bucharest, Romania*
† Electronic supplementary information (ESI) available. See DOI: https://doi.org/10.1039/d4cy01457j

the solvent through the development of "catch and release" catalytic systems. For instance, Zhou *et al.*[5] reported a pyrene-tagged chiral ligand for the *in situ* synthesis of a rhodium(I) complex that strongly adsorbed onto MWCNTs in ethyl acetate (93%) but only weakly in dichloromethane (50%). As an effect the asymmetric hydrogenation of α-dehydroamino esters in CH_2Cl_2 occurred under homogeneous conditions (conversion >99%, ee up to 96%) and in ethyl acetate under the heterogeneous ones affording efficient recycling (up to 9 runs).

Also, di-pyrene-functionalized complexes provided a stronger immobilization than mono-pyrene ones, as reported by Shi and co-workers for a rhodium(I) complex with two axially chiral MonoPhos ligands, each tagged with a pyrene moiety, onto the surface of graphene.[6a] The role of the solvent was again important as ethyl acetate allowed a strong adsorption of the complex onto graphene and catalytic performances comparable to those obtained under classical homogeneous conditions. Indeed, this supported catalyst showed very good activity and enantioselectivity (96% ee) for the asymmetric hydrogenation of dehydroamino acid derivatives as well as recyclability over 13 catalytic cycles and low Rh leaching (1.7%). Fernandez and co-workers investigated the π–π interaction between a rhodium complex and SWCNTs using a catch-and-release process monitored by UV-vis spectroscopy. Notably, their study revealed that the Rh complex/SWCNT nanocatalyst exhibited higher enantioselectivity compared to a non-supported complex. This enhanced selectivity is likely due to the improved exposure of the catalyst active site, demonstrating the potential of carbon nanotube-based supports in asymmetric catalysis.[6b]

As part of our continuing interest in heterogeneous enantioselective hydrogenation,[7] we report herein the synthesis of a pyrene-tagged rhodium complex as well as its non-covalent immobilization onto carbon nanotubes through a π–π stacking. We chose carbon nanotubes (CNTs) for their well-defined pores, large surface area, and low defect density, which enhance catalyst–support interaction. Their conductivity also helps dissipate heat in exothermic hydrogenation reactions, preventing hot spots that could affect catalyst stability and enantioselectivity.[7d] As ligand we selected a commercial **(2*S*,4*S*)-PPM** ligand because it proved particularly useful for the synthesis of new ligands covalently supported on different polymers,[8] silica,[9] or carbon nanotubes[7a] and also efficient for the immobilization of rhodium for the catalyzed asymmetric hydrogenation. With this aim, the synthesized **[Rh(COD)((2*S*,4*S*)-PPM-pyrene)]BF_4** novel complex was immobilized onto CNTs and then tested in the enantioselective hydrogenation of dimethyl itaconate (DMI) as a model substrate.

Experimental section

All commercially available reagents, *i.e.* dimethyl itaconate (99%, Sigma Aldrich), 1-pyrene butyric acid (Sigma Aldrich), 1-ethyl-3-(3-dimethylaminopropyl)carbodiimide (Sigma Aldrich), 4-dimethylaminopyridine (Aldrich), sodium hydroxide (NaOH) (pellets, purum, Chimica), and hydrochoric acid (HCl) (1N, VWR), were used as received. The anhydrous solvents: dichloromethane (DCM) and pentane were achieved from a Solvent Purification System (Innovative Technologies). Methanol (Carlo Erba) was used as received. H_2 (99.99%) and Ar (99.99%) were purchased from Linde.

Multi-walled carbon nanotubes (CNTs) were prepared by Chemical Vapor Deposition (CVD) using $AlFeCoO_4$ as the catalyst according to a previously described procedure.[10] Commercially available from Strem Chemicals, (2*S*,4*S*)-4-(diphenylphosphino)-2-[(diphenylphosphino)methyl] pyrrolidine (**(2*S*,4*S*)-PPM**) and bis(1,5-cyclooactadiene) rhodium(I)tetrafluoroborate were used as received.

Characterization techniques

The **(2*S*,4*S*)-PPM-pyrene** ligand and the **[Rh(COD)((2*S*,4*S*)-PPM-pyrene)]BF_4** complex were characterized using solution-state NMR spectroscopy. The experiments were conducted on Bruker spectrometers operating at 300 MHz and 600 MHz at the "Service RMN" facility of LCC-CNRS in Toulouse. Mass chromatograms of the ligand and complex were carried out on a TSQ 7000 Thermo Electron apparatus and electrospray (ES) on an API-365 MS/MS spectrometer (Perkin Elmer Sciex) using methane as a reacting gas.

CNTs and the CNT-immobilized **[Rh(COD)((2*S*,4*S*)-PPM-pyrene)]BF_4**) complex (abbreviated as **CNT@complex Rh** in the following text) were analyzed by a set of analyses. Fourier transformed infrared (FTIR) spectra were recorded in the 4000–400 cm^{-1} range using a Bruker Tensor II spectrometer equipped with a Harrick Praying Mantis diffuse reflection accessory. Raman spectroscopy analysis was carried out with a Horiba Jobin Yvon-Labram HR UV-visible-NIR Raman microscope with the excitation wavelength of 633 nm in the 150–4000 cm^{-1} spectral region. BET surface areas were measured using a Micromeritics ASAP2020 surface area and porosity analyzer. The samples were outgassed under vacuum for 24 h at 120 °C. The transmission electron microscopy (TEM) analyses were performed to study the immobilized **[Rh(COD)((2*S*,4*S*)-PPM-pyrene)]BF_4** complex after the deposition on a holey copper grid. TEM analyzes were performed with a JEOL JEM 1011 CX T electron microscope operating at 100 kV with a spot resolution of 4.5 Å and a JEOL JEM 1400 electron microscope operating at 120 kV.

CNT@complex Rh was analyzed by X-Ray Photoelectron Spectroscopy (XPS) using a Kratos AXIS Ultra DLD system equipped with a hemispherical analyzer with a reference intensity of over 50 000 counts per second (cps) and a spectral resolution of 0.6 eV, using Al K-alpha1 (1486.74 eV) radiation produced by a monochromatized X-ray source with a spot size of 0.7 mm. The operating power was 192 W (12 kV × 16 mA) and the spectra were recorded with a 160 eV pass energy for surveys and a 40 eV pass energy for high resolution measurements, with hybrid lens mode and slot aperture. The

partial charge compensation was achieved using a neutralizer flood gun (filament current of 1.8 A, charge balance of 2.7 V, filament bias of 1.02 V). The pressure in the analysis chamber was 10–9 mbar. The above parameters were optimized in order to fix the C 1s band of the carbon contamination at 284.60 ± 0.01 eV.

The loading of rhodium in **CNT@complex Rh** (1.82%) was determined by ICP-AES at Marion Technology. The sample was subjected to microwave-assisted dissolution in *aqua regia*. As the dissolution was partial, the mixture was subsequently filtered, and the ICP analysis was performed on the resulting filtrate using a Shimadzu ICP device. The Rh concentration was determined by analyzing three Rh spectral lines. Each reference was analyzed in duplicate (N = 2), and the reported results represent the average of both measurements.

Synthesis of the (2*S*,4*S*)-PPM-pyrene ligand

To a solution of **(2*S*,4*S*)-PPM** (250 mg, 0.55 mmol) in 6 ml of dry DCM, 1-pyrene butyric acid (206 mg, 0.72 mmol), 4-dimethylaminopyridine (28 mg, 0.22 mmol) and 1-ethyl-3-dimethylaminopropylcarbodiimide (127 mg, 0.66 mmol) were added. The reaction mixture was stirred at RT for 24 h under argon. Subsequently, the reaction mixture was concentrated under vacuum. The resulting yellow viscous residue was purified through an acid–base washing with 1 M HCl and then with 1 M NaOH degassed solutions. The organic phases were dried over magnesium sulfate ($MgSO_4$) and the solvent was evaporated. The **(2*S*,4*S*)-PPM-pyrene** ligand was obtained as a light-yellow solid (290 mg, yield = 72%).

$^{31}P\{^1H\}$ NMR (298 K, CD_2Cl_2, 121 MHz); δ (ppm): major conformer: δ −23.41 (s, P^1), −9.58 (s, P^2); minor conformer: −22.93 (s, P^1), −7.05 (s, P^2).

MS (DCI-CH_4): 724.29 (M + H), HRMS (DCI-CH_4): calculated for $C_{49}H_{43}NO_3P$ (diphosphine dioxide) 755.2718, found 755.2706.

Synthesis of [Rh(COD)((2*S*,4*S*)-PPM-pyrene)]BF_4

A solution of **(2*S*,4*S*)-PPM-pyrene** ligand (150 mg, 0.20 mmol) in 5 ml of dry DCM was transferred *via* a cannula to a solution of bis(1,5-cyclooctadiene)rhodium(I)tetrafluoroborate (98 mg, 0.20 mmol) in dry DCM solvent (5 mL) under argon. The resulting reaction mixture was stirred for 24 h under argon at RT. The product was then precipitated with dry pentane, filtered, and dried under vacuum resulting as a yellow solid (170 mg, yield = 91%). As confirmed by ^{31}P NMR the Rh-complex presented both major and minor conformers. $^{31}P\{^1H\}$ NMR (298 K, CD_2Cl_2, 121 MHz); δ (ppm): major conformer: 15.04 (dd, J_{P-P} = 37.2 Hz, J_{P-Rh} = 140.0 Hz, P^1), 43.4 (dd, J_{P-P} = 37.6 Hz, J_{P-Rh} = 145.1 Hz, P^2), minor conformer: 15.42 (dd, J_{P-P} = 37.3 Hz, J_{P-Rh} = 141.8 Hz, P^1), 45.58 (dd, J_{P-P} = 37.1 Hz, J_{P-Rh} = 144.5 Hz, P^2).

MS (ESI): 934 $[M\text{-}BF_4]^+$.

Immobilization of the chiral [Rh(COD)((2*S*,4*S*)-PPM-pyrene)]BF_4 onto the CNT surface

A suspension of CNTs (200 mg) in MeOH (4 ml) was maintained under ultrasonication for 30 min. Then a solution of **[Rh(COD)((2*S*,4*S*)-PPM-pyrene)]BF_4** (45 mg, yellow) in MeOH (4 ml) was added *via* a cannula under argon. The reaction mixture was stirred for 24 h at RT. The immobilized complex was then filtered with MeOH until a colorless filtrate was obtained before drying under vacuum for 20 h.

Asymmetric hydrogenation with the immobilized Rh complex

Hydrogenation reactions with the immobilized Rh complex were performed in a stainless-steel autoclave, using 0.16 g (1 mmol) of dimethyl itaconate, 0.06 g of **CNT@complex Rh** that corresponds to 1.09 mg of Rh (0.0105 mmol) and 4 mL of MeOH. The reactor was pressurized with H_2 to 5.5 bar and the reaction mixture was stirred (1100 rpm) at RT for a determined time. After the reaction, the hydrogen pressure was carefully released and the catalyst was recovered *via* filtration under nitrogen and then washed with fresh solvent.

Conversion and enantiomeric excess (ee) of the product was determined on a Perkin Elmer Clarus 500 chromatograph equipped with a chiral column, Beta DEX™ 225 (30 m × 0.25 mm × 0.25 μm), using decane as an internal standard. The retention times for the produced methyl succinate were 7.9 and 8.3 min for the (*S*) and (*R*) forms, respectively, and 11.5 min for dimethyl itaconate.

Results and discussion

Synthesis of the [Rh(COD)((2*S*,4*S*)-PPM-pyrene)]BF_4 complex

The complex synthesis was carried out in two steps starting from the commercially available (2*S*,4*S*)-4-(diphenylphosphino)-2-[(diphenyl-phosphino)-methyl] pyrrolidine and **(2*S*,4*S*)-PPM** molecule. Firstly, a simple amide coupling reaction between **(2*S*,4*S*)-PPM** and 1-pyrenebutyric acid in the presence of 4-dimethylaminopyridine (DMAP) and 1-ethyl-3-(3 dimethylaminopropyl)carbodiimide (EDC) (dry DCM, RT, 24 h, argon) allowed to introduce a pending pyrene group in the skeleton of **(2*S*,4*S*)-PPM** for a further interaction with the surface of CNTs (Scheme 1).

The **(2*S*,4*S*)-PPM-pyrene** ligand, obtained as light-yellow solid (yield = 72%), was fully characterized by $^{31}P\{^1H\}$-NMR, ^1H-NMR, ^{13}C-NMR, and high-resolution mass spectrometry. The $^{31}P\{^1H\}$ NMR spectrum showed two sets of singlets in a 75/25 ratio (major species: δ = −23.41 (s, P^1), −9.58 (s, P^2);

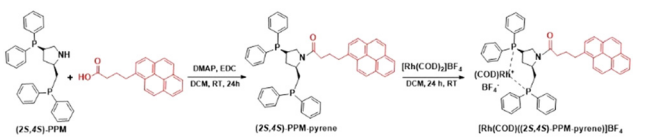

Scheme 1 Synthesis of the **(2*S*,4*S*)-PPM-pyrene** ligand and **[Rh(COD)((2*S*,4*S*)-PPM-pyrene)]BF_4** complex.

minor species: δ = −22.93 (s, P^1), −7.05 (s, P^2)) evidencing the formation of two species (see the ESI,† Fig. S1). These two species could be ascribed to two conformational isomers in equilibrium in solution at RT due to the slow rotation of the pyrene moiety around the N–(CO) bond as previously observed for the *tert*-butoxycarbonyl group in the (2*S*,4*S*)-*N*-(*tert*-butoxycarbonyl)-4-(diphenylphosphino)-2-[(diphenylphosphino)-methyl] ligand, (2*S*,4*S*)-BPPM.[11] Complementary ^{1}H and ^{13}C NMR experiments were used to assign the protons and carbons of each conformer, including those of the pyrene group (see the ESI,† Fig. S2–S6).

In a second step, the reaction of bis(1,5-cyclooctadiene) rhodium(I)tetrafluoroborate with one equivalent of the **(2*S*,4*S*)-PPM-pyrene** ligand in dichloromethane quantitatively led to the cationic complex **[Rh(COD)((2*S*,4*S*)-PPM-pyrene)]BF_4**. As previously observed for the ligand **(2*S*,4*S*)-PPM-pyrene**, $^{31}P\{^1H\}$ NMR analysis revealed two sets of doublets of doublets in a nearly 75/25 ratio indicating the presence of two different species; major species: δ = 15.04 (dd, $J_{P^1-P^2}$ = 37.2 Hz, J_{P^1-Rh} = 140.0 Hz, P^1), 43.40 (dd, $J_{P^1-P^2}$ = 37.6 Hz, J_{P^2-Rh} = 145.1 Hz, P^2), minor species: δ = 15.42 (dd, $J_{P^1-P^2}$ = 37.3 Hz, J_{P^1-Rh} = 141.8 Hz, P^1), 45.58 (dd, $J_{P^1-P^2}$ = 37.1 Hz, J_{P^2-Rh} = 144.5 Hz, P^2) (see the ESI,† Fig. S7–S9, respectively). These results clearly confirmed the complexation of each conformer of the **(2*S*,4*S*)-PPM-pyrene** ligand at the rhodium center as in the case of the coordination of the BPPM ligand on the same rhodium precursor.[11]

Immobilization of [Rh(COD)((2*S*,4*S*)-PPM-pyrene)]BF_4 *via* non-covalent π–π interactions

Immobilization of the **[Rh(COD)((2*S*,4*S*)-PPM-pyrene)]BF_4** complex onto the CNT surface (Scheme 2) was achieved by mixing the CNT support and the complex in MeOH under argon, by considering a theoretical deposition of a Rh wt of 2%. After sonication of the suspension for 30 min and 24 h of stirring at RT, the solid was filtered off, washed with MeOH and vacuum-dried for 20 h. The use of MeOH enabled an efficient adsorption of the complex onto the CNTs as observed by the color of the filtrate after washing. The colorless testified a low concentration of the yellow complex in the filtrate if any (see the ESI,† Fig. S10). Actually, the effective adsorption was confirmed by ICP-AES analysis on the immobilized complex, which indicated a rhodium content onto the CNTs of 1.82%, which is very close to the theoretical value.

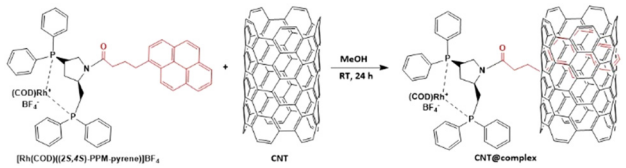

Scheme 2 Immobilization of the **[Rh(COD)((2*S*,4*S*)-PPM-pyrene)]BF_4** complex onto CNTs.

Characterization of the CNT-immobilized complex (CNT@complex Rh)

For the CNTs, FTIR analysis indicated absorption bands characteristic of the CNT skeleton with C=C plane vibration at 1630 cm^{-1}. **CNT@complex Rh** presented additional bands at 1580 cm^{-1} (C–N stretching), at 1690 cm^{-1} (amide C=O stretching), at 1040 cm^{-1} (P–N–C asymmetric stretching), at 1258 cm^{-1} (C–H skeletal vibrations), at 1390 cm^{-1} (C–N–C deformation) and at 2960 cm^{-1} (asymmetric C–H stretching) attributed to the skeleton of the ligand (see ESI,† Fig. S11).

The Raman spectra of the CNTs and **CNT@complex Rh** indicated no major differences after the immobilization of the Rh complex. The signals at ~1330 cm^{-1} (D line) relate to the presence of the defects, while those at ~1570 cm^{-1} (G line) account for a graphitic arrangement. The intensity ratio of the D and G signals serves as an indicator of defects and graphitic arrangement,[12] a lower I_D/I_G ratio indicating a lower quantity of defects. Comparison of the I_D/I_G ratio of initial CNTs (1.23) and **CNT@complex Rh** (1.20) indicated no significant change in the defects of the CNTs, as expected (see the ESI,† Fig. S12).

The TEM analysis of the **CNT@complex Rh** revealed the absence of nanoparticles or rhodium agglomeration (Fig. 1).

Textural characterization of **CNT@complex Rh** was performed by BET through the N_2 adsorption–desorption analysis (see the ESI,† Fig. S13). The BET area for **CNT@complex Rh** was 86 $m^2\ g^{-1}$ against 211 $m^2\ g^{-1}$ for the raw CNT material. Carbon nanotubes are known to be mainly mesoporous materials, as their porosity comes from the inner cavity of the nanotube and pores formed by the interaction of isolated nanotubes. The decrease in porosity observed may arise from a change in the surface properties of the CNTs by the adsorption of the Rh complex at their surface, making the spaces between the CNTs different due to steric hindrance, which could impact the porosity.

XPS analysis identifies the binding energies corresponding to the oxidation states of the major elements in the **CNT@complex Rh** (C, O, P, Rh) (see the ESI,† Fig. S14 and S15). An additional band attributed to Fe was also observed that corresponds to the residual iron catalyst used for the synthesis of the CNTs. XPS spectra revealed C 1s peaks of high intensity located at 284.6 eV (graphitic carbon, sp^2-carbon), 285.3 eV (aliphatic C–C=O, sp^3-carbon), 286.3 eV (carbon in keto–enolic form), and 287 eV (keto group). These

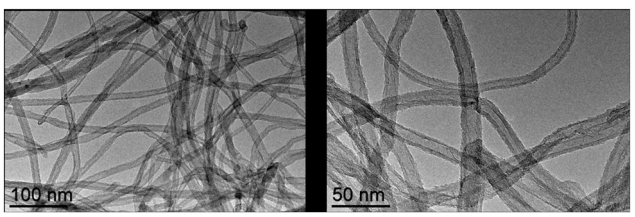

Fig. 1 TEM images of **CNT@complex Rh** at two different magnifications.

functionalities were also confirmed by the intensity of the O 1s peaks located at 531.7 eV (C═O), 533.3 eV (C–O of ester) and 536.0 eV (oxygen of water).[13] Binding energies in the range of 130.8–132.8 eV, corresponding to the P 2p level, were also observed and were attributed to phosphorus attached to phenyl groups in the organo-phosphorus compounds. The binding energy for the N 1s level was found at 400.0 eV, corresponding to nitrogen in the pyridonic or pyrrolic form. Finally, the low-energy corresponding to the Rh $3d_{5/2}$ and Rh $3d_{3/2}$ photoelectron pair at 309.6 and 313.8 eV, respectively, is consistent with the presence of the Rh(I) 3d photoelectrons.[7a] A second Rh $3d_{5/2}$ and Rh $3d_{3/2}$ photoelectron signal pair, at 310.5 and 315.0 eV is assigned to the Rh(III) 3d photoelectrons.[14] The presence of Rh(III) species may rely from either the oxidation of the sensitive Rh complexes before XPS analysis as they were shortly exposed to air. No signal of Rh(0) has been detected. The Rh/P ratio for the **CNT@complex Rh** was found to be 0.52, which is close to the theoretical value (0.5) (see ESI,† Table S1).

All these analyses confirmed the maintained integrity of the complex after the immobilization onto CNTs.

Asymmetric hydrogenation of dimethyl itaconate in the presence of CNT@complex Rh

The catalytic efficiency and the recyclability of **CNT@complex Rh** were tested in the enantioselective hydrogenation of dimethyl itaconate (DMI). For a comparison purpose, a series of catalytic tests were firstly performed under homogeneous conditions using the unsupported [Rh(COD)((2*S*,4*S*)-BPM)]BF_4 (ref. 15) and **[Rh(COD)((2*S*,4*S*)-PPM-pyrene)]BF_4** complexes as catalysts. In both cases, the hydrogenation (in MeOH, at RT, under 5.5 bar of hydrogen) occurred with very high rates (complete conversion in 30 min) and good enantioselectivities towards (*S*)-methyl succinate (72 and 57%, respectively) (Table 1, entries 1–2). These initial tests allowed us to conclude that the enantioselectivity of the Rh complex is affected by the presence of the pyrene tag.

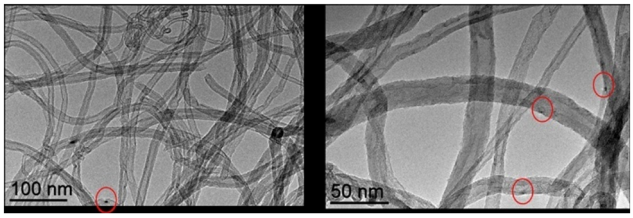

Fig. 2 TEM images of the spent **CNT@complex Rh** catalyst at two different magnifications.

Then, the catalytic tests were carried out with the immobilized Rh complex (**CNT@complex Rh**). The blank test conducted under the same reaction conditions in the presence of the CNTs showed that no hydrogenation of DMI occurred, confirming the inertness of the CNT support for this reaction (Table 1, entry 3). **CNT@complex Rh** afforded a low activity (29% conversion after 4 h at RT) and a moderate enantioselectivity for the hydrogenation of dimethyl itaconate (34% ee towards (*S*)-methyl succinate (Table 1, entry 4)) (see the ESI,† Table S2). These results indicated that the immobilization of the Rh complex onto the CNTs led to a decrease of both the conversion and enantiomeric excess, evidencing an interference of the support on the course of the reaction, which can rely from less accessible active sites and/or modification of the geometry of the ligand. Increasing the reaction time to 7 h resulted in a better conversion of the substrate (74%) with almost the same enantioselectivity (34% ee) (Table 1, entry 6). The catalyst was then separated from the reaction mixture by filtration and washed with MeOH. Interestingly, no Rh leaching was detected by ICP-AES analysis in the obtained liquid phase, which demonstrated the absence of soluble Rh species and further the heterogeneous nature of catalysis. Finally, a complete conversion of DMI was obtained after 15 h with a fairly similar enantioselectivity (Table 1, entry 7 *vs.* entries 4 and 6), suggesting a good stability of the catalyst over time under the catalytic conditions applied.

Table 1 Catalysis results for the enantioselective hydrogenation of dimethyl itaconate by free Rh complexes and the CNT-immobilized Rh complex[a]

Entry	Catalyst	S/Rh	Time (h)	Conversion[b] (%)	ee[b] (%) (*S*)
	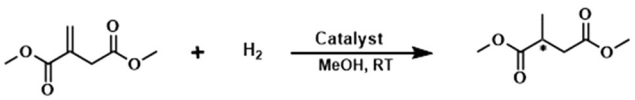				
1	**[Rh(COD)((2*S*,4*S*)-BPPM)]BF_4**	80	0.5	100	72
2	**[Rh(COD)((2*S*,4*S*)-PPM-pyrene)]BF_4**	80	0.5	100	57
3	CNT	—	24	0	—
4	**CNT@complex Rh**	95	4	29	34
5[c]	**CNT@complex Rh**	95	4	26	28
6	**CNT@complex Rh**	95	7	74	34
7	**CNT@complex Rh**	95	15	100	29

[a] Reaction conditions: 0.16 g of substrate, 0.0099 g of [Rh(COD)((2*S*,4*S*)-BPPM)]BF_4, 0.012 g of **[Rh(COD)((2*S*,4*S*)-PPM-pyrene)]BF_4**, and 0.060 g of immobilized Rh-complex, 5.5 bar of H_2, 4 ml of MeOH, RT. [b] Determined by chiral GC using a Beta DEX™ 225 column. [c] Recycling of entry 4.

The recyclability of the **CNT@complex Rh** was evaluated as well. The second catalytic run afforded a conversion and an enantiomeric excess quite similar to those obtained in the initial run (Table 1, entry 4 *vs.* entry 5).

The spent **CNT@complex Rh** of the second catalytic run (Table 1, entry 5) was characterized by IR, XPS and TEM. The FTIR displayed no discernible alteration in either the intensity or the positioning of the absorption bands when compared to the spectra of the fresh **CNT@complex Rh** (see the ESI,† Fig. S16). XPS analysis indicated no change in the rhodium oxidation state, *i.e.* no Rh(0) species[16] was detected for this material as no band at binding energy below 308 eV was observed (see the ESI,† Fig. S17). However, TEM analysis of the spent catalyst showed a few black dots that could correspond to small Rh NPs (size between 1 and 3 nm, highlighted by red circles in Fig. 2). The observation of only a few Rh nanoparticles indicated that only a low part of the rhodium complex has been reduced, which can explain why no Rh(0) was detected by XPS.

Conclusions

A new chiral rhodium complex, Rh-(2*S*,4*S*)-PPM-pyrene (**complex Rh**), containing a diphosphine ligand with a pyrene tag has been synthesized. This complex was successfully anchored on the surface of CNT by π–π stacking under mild conditions, yielding **CNT@complex Rh**. This chiral heterogeneous Rh complex was characterized by a set of analytical techniques and tested for the asymmetric hydrogenation of the dimethyl itaconate as the prochiral substrate. Although **CNT@complex Rh** exhibited a reduced activity and enantioselectivity compared to its free counterpart, this catalyst demonstrated a good stability after recycling.

Substantial improvements in enantioselectivities and catalytic activities could be achieved by simply changing the chiral pyrene-tagged diphosphine ligand and/or the prochiral substrates.

In summary, we have developed an efficient method for the immobilization of metal complexes onto carbon nanotubes by π–π interaction. This work opens up prospects for developing other heterogeneous hybrid chiral catalysts for enantioselective hydrogenation and may be for other asymmetric reactions.

Data availability

Most of the data of our work are present in the manuscript or in the ESI.† Moreover, when our work is accepted for publication, the source data will be deposited as annex in the "HAL" Repository, in the form of a ZIP archive following the Open Air and F.A.I.R. data principles.

Author contributions

Z. A. performed the syntheses and catalytic studies and contributed to material characterization. V. I. P., K. P., J. D., and M. G. conceived, coordinated and supervised the work. All authors contributed to the writing of the manuscript. All authors have read and agreed to the published version of the manuscript.

Conflicts of interest

The authors declare no conflict of interest.

Acknowledgements

This work has received funding from the European Union's Horizon 2020 research and innovation program under the Marie Skłodowska-Curie grant agreement No. 860322 for the ITN-EJD "Coordination Chemistry Inspires Molecular Catalysis" (CCIMC). We are grateful to the CNRS (Centre National de la Recherche Scientifique), the INP-ENSIACET (Institut National Polytechnique de Toulouse) and the University of Bucharest for providing access to facilities. The authors warmly thank the technical assistance provided by Vincent Collière (LCC-CNRS, Toulouse) for TEM analyses, Popescu Dana (University of Bucharest) for XPS analyses and Jérôme Esvan (CIRIMAT, Toulouse) for fruitful scientific discussions. The Raimond Castaing Micro-characterization Center (UAR 3623, Toulouse) is also thanked for the access to electron microscopes.

References

1 (*a*) J. M. Fraile, J. I. Garcia and J. A. Mayoral, *Chem. Rev.*, 2009, **109**, 360–417; (*b*) L. Zhang, S. Luo and J. P. Cheng, *Catal. Sci. Technol.*, 2011, **1**, 507–516; (*c*) A. N. Marianov, Y. Jiang, A. Baiker and J. Huang, *Chem Catal.*, 2023, **3**, 100631; (*d*) H. Zhang, S. Liu, Q. Zhang, K. Hong, J. Li, X. Yan and J. Pan, *ChemistrySelect*, 2025, **10**, e202405224; (*e*) P. Lakhani and C. K. Modi, *Mol. Catal.*, 2023, **548**, 113429; (*f*) M. S. Shukla, P. E. Hande and S. Chandra, *ChemistrySelect*, 2022, **7**, e202200549; (*g*) A. Franco and E. Baráth, *ChemCatChem*, 2025, **17**, e202400019.

2 L. Ibos and E. Schulz, *C. R. Chim.*, 2024, **27**, 57–83.

3 C. C. Gheorghiu, C. Salinas-Martínez de Lecea and M. C. Román-Martínez, *Appl. Catal., A*, 2014, **478**, 194–203.

4 M. Rufete-Beneite and M. C. Román-Martínez, *Eur. J. Inorg. Chem.*, 2021, **2021**, 223–225.

5 L. Xing, J. Xie, Y. Chen, L. Wang and Q. Zhou, *Adv. Synth. Catal.*, 2008, **350**, 1013–1016.

6 (*a*) E.-J. Hao, G.-X. Li, Z.-Z. Lv, F.-S. Li, Y.-Q. Chen, S.-J. Lin, C.-Z. Shi and L. Shi, *Org. Chem. Front.*, 2020, **7**, 345–349; (*b*) J.-F. Moya, C. Rosales, I. Fernández and N. Khiar, *Org. Biomol. Chem.*, 2017, **15**, 5772–5780.

7 (*a*) C. C. Gheorghiu, B. F. Machado, C. Salinas-Martínez de Lecea, M. Gouygou, M. C. Román-Martínez and P. Serp, *Dalton Trans.*, 2014, **43**, 7455–7463; (*b*) A. Negoi, B. Cojocaru, V. I. Parvulescu, N. Imlyhen and M. Gouygou, *Mol. Catal.*, 2019, **474**, 110420; (*c*) Z. Arora, M. Rais, V. I. Parvulescu, K. Philippot, J. Durand and M. Gouygou, *ChemNanoMat*, 2024, e202400125; (*d*) M. R. Axet, O. Dechy-Cabaret, J.

Durand, M. Gouygou and P. Serp, *Coord. Chem. Rev.*, 2016, **308**, 236–345.
8 (*a*) T. Malmström and C. Andersson, *Chem. Commun.*, 1996, 1135–1136; (*b*) D. J. Gravert, A. Datta, P. Wentworth and K. D. Janda, *J. Am. Chem. Soc.*, 1998, **120**, 9481; (*c*) T. Malmström, *J. Mol. Catal. A: Chem.*, 1999, **139**, 259–270.
9 B. Pugin, *J. Mol. Catal. A: Chem.*, 1996, **107**, 273–279.
10 A. Morançais, B. Caussat, Y. Kihn, P. Kalck, D. Plee, P. Gaillard, D. Bernard and P. Serp, *Carbon*, 2007, **45**, 624–635.
11 I. Ojima, T. Kogure and N. Yoda, *J. Org. Chem.*, 1980, **45**, 4728–4739.
12 Z. Lin, T. Le, X. Song, Y. Yao, Z. Li, K. Moon, M. M. Tentzeris and C. Wong, *J. Electron. Packag.*, 2013, **135**, 011001.
13 J. L. Figueiredo and M. F. R. Pereira, *Catal. Today*, 2010, **150**, 2–7.
14 Y. Okamoto, N. Ishida, T. Imanaka and S. Teranishi, *J. Catal.*, 1979, **58**, 82–94.
15 M. J. Burk and M. F. Gross, *Tetrahedron Lett.*, 1994, **35**, 9363–9366.
16 C. J. Powell, *J. Electron Spectrosc. Relat. Phenom.*, 2012, **185**, 1–3.